Turkish Journal of Electrical Engineering & Computer Sciences

http://journals.tubitak.gov.tr/elektrik/

Research Article

Turk J Elec Eng & Comp Sci
(2015) 23: 1242 – 1256

doi:10.3906/elk-1212-157

3D imaging for ground-penetrating radars via dictionary dimension reduction

Muhammed DUMAN, Ali Cafer GÜRBÜZ*
Department of Electric and Electronics Engineering, TOBB University of Economics and Technology, Ankara, Turkey

Received: 26.12.2012 • **Accepted/Published Online:** 02.05.2013 • **Printed:** 28.08.2015

Abstract: Ground-penetrating radar (GPR) has been widely used in detecting or imaging subsurface targets. In many applications such as archaeology, utility imaging, or landmine detection, three-dimensional (3D) images of the subsurface region is required for better understanding of the sensed medium. However, a high-resolution 3D image requires wideband data collection both in spatial and time/frequency domains. Match filtering is the main tool for generating subsurface images. Applying match filtering with the data acquisition impulse response for each possible voxel in the 3D region with the collected data requires both a tremendous amount of computer memory and computational complexity. Hence, it is very costly to obtain 3D GPR images in most of the applications although 3D images are very demanded results. In this paper, a new 3D imaging technique is proposed that will first decrease the memory requirements for 3D imaging with possible implications for less computational complexity. The proposed method uses the shifted impulse response of the targets that are on the same depth as a function of scanning position. This similarity of target responses for data dictionaries for only 2D target slices is constructed with twice the length in scanning directions and this 2D dictionary is mainly used for generating 3D images. The proposed method directly saves memory due to dimension reduction in dictionary generation and also decreases computational load. Simulation results show generated 3D images with the proposed technique. Comparisons in both memory and computational load with the standard backprojection show that the proposed technique offers advantages in both areas.

Key words: Ground penetration radar, 3D imaging, high dictionary size, computational load, dimension reduction

1. Introduction

Ground-penetrating radar (GPR) [1–3] has become an important technology in recent years due to its broad applications in both military and civilian sectors. Traditional GPRs image the subsurface by transmitting short electromagnetic pulses or a train of subpulses with stepped carrier frequencies and process the reflections caused by permittivity discontinuities in the ground. GPRs can detect anything with dielectric contrast like permittivity to the surrounding medium. Because of this wide applicability they are used in landmine detection [4,5], environmental and archaeological investigations [6,7], through-the-wall imaging and detection [8,9], and civil applications [10,11]. Imaging with GPR requires the formation of a synthetic aperture, which is done by scanning a GPR sensor over the region of interest and recording the time/frequency signal returns for many spatial positions.

In many applications the demand is towards obtaining 3D and high-resolution images of the medium. This operation requires a very large amount of space-time/frequency data since high resolution in this range

*Correspondence: acgurbuz@etu.edu.tr

requires ultrawideband pulses and resolution in cross ranges requires longer synthetic apertures. Despite this fact, 3D imaging in GPR is applied often in the literature. In [12], an overview of various aspects of using GPR in archaeology was presented. The advantages of modeling were explained and presented with the range of possible applications in four case histories, ranging from a survey of a lake to a 3D model of a part of a Roman town. In some GPR surveys, sites containing continuous linear features extending over several meters in length such as foundations, ditches, walls, or roads are imaged. Most archaeological surveyors have not yet pushed GPR to its full potential and experienced the benefits of maximum resolution achieved with very dense data acquisition and processing, but interesting 3D visualization research was proposed in [13]. In [14] 3D imaging in geophysical structures was presented. Imaging of 3D bodies in mine detection and nondestructive testing applications was used in [15].

The increasing need for detailed 3D imaging of the shallow subsurface and the higher horizontal and vertical resolution required in many applications make 3D GPR one of the most important current research topics. In GPR imaging match filtering-based backprojection [16] is the most commonly applied idea to obtain an image. For 3D imaging backprojection is applied by synthesizing the model data for each voxel point in the discretized 3D volume and correlating the measured data with this synthesized data model or data acquisition impulse response for each voxel to be imaged. This model data can be created only once and stored in memory, but this requires a huge memory size even for moderate size 3D images and resolution steps. The model data can also be synthesized on the fly, but then the computational complexity of the technique increases dramatically, requiring high-speed parallel CPUs and expensive data processing packages. Hence, most GPR imaging applications still generate data by means of 1D and 2D techniques.

To present a solution for the disadvantages of 3D imaging and especially to decrease the computational complexity of the imaging algorithms, an important amount of research has already been done. One of the main techniques in faster 3D imaging is to use fast Fourier transform (FFT) in imaging stages. The imaging algorithm in [17] is one of the methods that functions in the frequency domain. Hence for this method, the data should be acquired in the frequency domain or transformed to it. Still, 3D dictionaries should be used, but using FFT in the inherent calculations makes it faster compared to the standard backprojection method. In [18], an algorithm for computation of the scattered fields from 3D inhomogeneous dielectric scatterers was presented. In this method, Galerkin's testing formulation of an integral equation for 3D electromagnetic fields is represented by a multiinput and multioutput linear system with known kernels. On a regular grid with rooftop basis functions, the kernels are discretized and accurately evaluated. Furthermore, they are represented by Toeplitz matrices, which reduces the storage and computational complexity in solving for the scattered fields.

Another faster 3D imaging technique is to use quadtree imaging, which applies a multilevel resolution scheme as shown in [19,20]. In this method, the 3D volume to be imaged is divided into 8 subvolumes at each stage of the quadtree algorithm. The energy intensity or the pixel value for each of these subvolumes is calculated. In the following iterations of the algorithm finer resolutions are obtained and potential target subvolumes get higher intensity values as that of the background noise decreases. Subdivision of some volumes can be buried if it is decided that there is no target in the volume in the previous iteration. Hence, possible target areas are explored further with finer resolutions while clutter or noise regions are not explored, resulting in savings in computational complexity.

In addition to these techniques, another significant research area is sparse reconstruction and compressive sensing. Recent results in the theory of compressive sensing (CS) [21–24] show that reconstruction of unknown signals, which have a sparse representation in a certain transformation domain, can be obtained from a much

smaller set of measurements as compared to conventional techniques. If GPR applications admit a sparse representation, reconstruction of target scenes can be formulated as a sparse signal reconstruction problem. Application of CS to a GPR imaging problem was first demonstrated in [25]. In that work, the subsurface area was modeled to consist of a small number of discrete point-like targets and a dictionary of model data was generated for each possible discrete target point. The subsurface image was generated by solving an ℓ_1 minimization-based optimization problem with a decreased number of measurements. Later, these results were extended to the stepped frequency [26] and impulse GPR [27] cases. In [28], Yoon, et al. used CS for through-the-wall imaging using wide-band beamforming, where the unmeasured frequency points were reconstructed with CS and conventional wideband beamforming was applied on the reconstructed measurements. In all of these works CS-based imaging provides the obtaining of less measurement, possibly both in the space and time/frequency domains. Decreasing the number of measurements acquired provides advantages both in data acquisition times and total memory requirements. On the other hand, CS-based imaging is only advantageous if the target space is sparse and it requires the data dictionary to be constructed before the imaging. The CS-based imaging actually requires a solution of a sparsity-enhanced optimization problem, which requires matrix inverses at each optimization step and is practically much more computationally complex compared to standard match filtering-based techniques and totally impractical for moderate-resolution 3D GPR imaging problems.

The CS imaging technique is advantageous in terms of data acquisition time, but since convex optimization takes too much time, this advantage is lost. If the imaging area is large or fine resolution in imaging is used, or if a 3D volume is going to be imaged, the algorithm starts to become unpractical. Mainly because of the computational complexity of convex optimization, faster greedy techniques are pursued. One example of these is orthogonal matching pursuit (OMP) [29], which is a suboptimal sparse solver. Although these suboptimal solvers do not guarantee any globally optimal solution, they are computationally more efficient. An example application of using OMP for GPR imaging was presented in [30]. OMP uses the same dictionary as CS but iteratively removes the most correlated part of the measurement at each iteration. Hence, it uses a simpler dictionary with a reduced number of measurements but applies several match filterings until converging.

Sparsity-based techniques offer great advantages such as decreasing number of measurements, high resolution, and less cluttered images, but they require comparably higher computational complexity. To decrease their computational load, mainly the dictionary sizes should be decreased without losing imaging performance. In [31], it was shown that the underlying propagation model leads to a block-Toeplitz structure [32] in two of the dimensions, which can be exploited to reduce both the storage and computational complexity. Thus, it is shown that a reduction by three orders of magnitude in computational resources for the CS problem will make 3D imaging applications feasible. Although CS-based techniques offer good advantages, they are limited with sparse images.

This paper presents a new approach based on data modeling symmetry in the scanning direction of GPR, which leads to decreased dimension of dictionaries and allows using 2D dictionaries instead of huge 3D ones for obtaining 3D images with efficient computational ideas. Figure 1 shows the data model of a two target 2D slice as the GPR scans in one direction. It is observed from the space-time domain data that the responses for each target are actually shifted versions of each other since the targets are at the same depth. This additional information is used to decrease one dimension of the data and leads to more efficiency both in terms of memory and computational complexity. Although this method offers advantageous solutions to CS-based problems, the technique itself does not assume any prior sparsity requirement and hence can be used in a general 3D imaging setting. An initial version of this idea was presented in [33].

The paper is organized as follows. Data acquisition types are briefly introduced in Section 2 for GPR and

Section 3 details several state-of-the-art GPR imaging techniques. The proposed imaging method is presented in Section 4. Section 5 presents the simulation results with memory and computation load comparisons. Conclusions are drawn in Section 6.

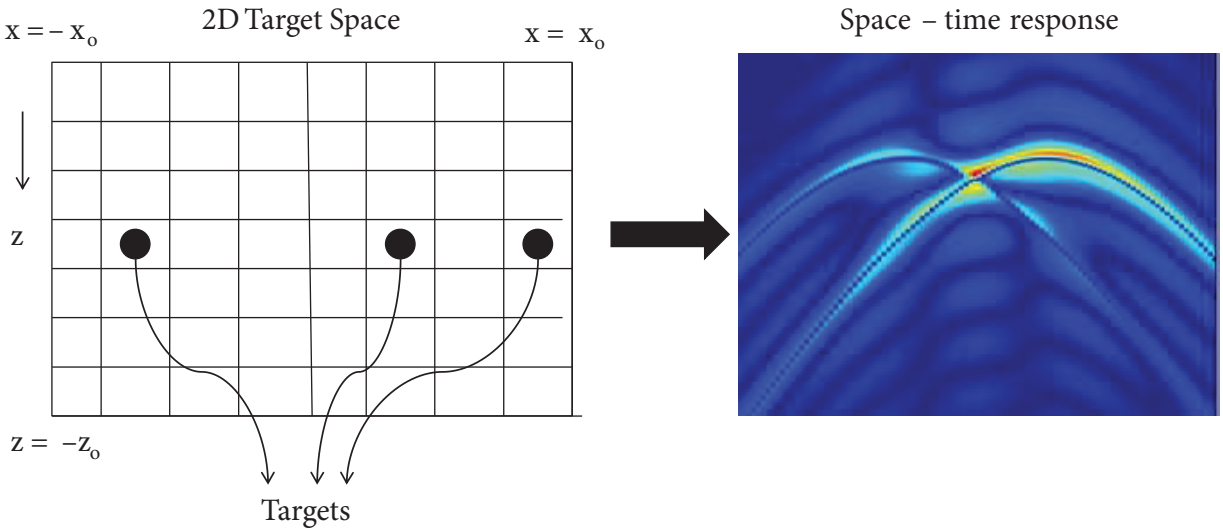

Figure 1. Data acquisition responses for targets at the same depth along the data scanning direction are shifted versions of each other in the scan direction.

2. GPR data acquisition

GPR data can be collected and displayed in a number of different formats. These are generally represented as a one-, two-, or three-dimensional dataset, denominated by the acoustic terminology A-, B- and C- scans [34]. Each presentation mode provides a different way of looking at and evaluating the sensed medium.

A single data waveform d (x_i, y_j, t) recorded with the antennas at a fixed scan position (x_i, y_j) is referred to as an A-scan. An example A-scan for GPR is shown in Figure 2. Since the scan position is a fixed A-scan it is a function of only time and the time delay is related with the depth of the target. A-scans and their energies are generally used for target detection tests at the corresponding scan positions.

If the GPR antennas are moved along one direction (scanning direction) on a line, one can gather a set of A-scans, which forms a two-dimensional data set. The collection of A-scans along the x-axis for a fixed y_j scan position as shown in Figure 3 forms the B-scan data. B-scan GPR data are generally shown as two-dimensional images and mainly represent a vertical slice of data in the ground. Figure 3a shows a representation of a GPR B-scan data. Figure 3b shows a B-scan image with a hyperbolic response due to a single point reflector.

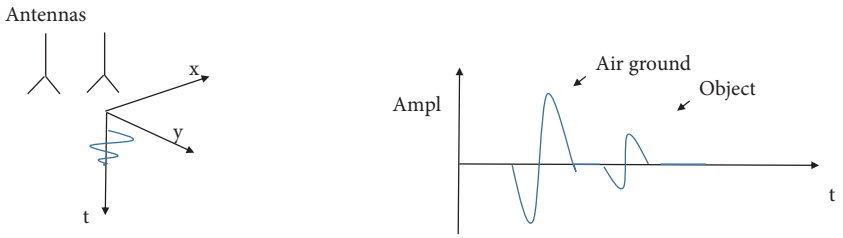

Figure 2. Representation of a GPR A-scan data [34].

This hyperbolic response can be easily obtained by the geometry of the scanning system. It is important to note that this hyperbolic response due to a single target will shift in the scanning direction if the x-position of the target also shifts. The shape of the hyperbola is the same for targets at the same depth but shape changes with depth. The hyperbola becomes more flat for deeper targets. The main goal of imaging or migration procedures is to invert back the hyperbolic responses to single points.

Finally, a collection of multiple parallel B-scans forms the C-scan data. Hence, if the GPR antenna is moved in the x-y-plane over a regular grid the collected data d (x, y, t) forms the C-scan data. An example C-scan is shown in Figure 4. For 3D image formation C-scan data are required to be acquired. The next section details the standard 3D imaging algorithms assuming that this type of C-scan data is collected.

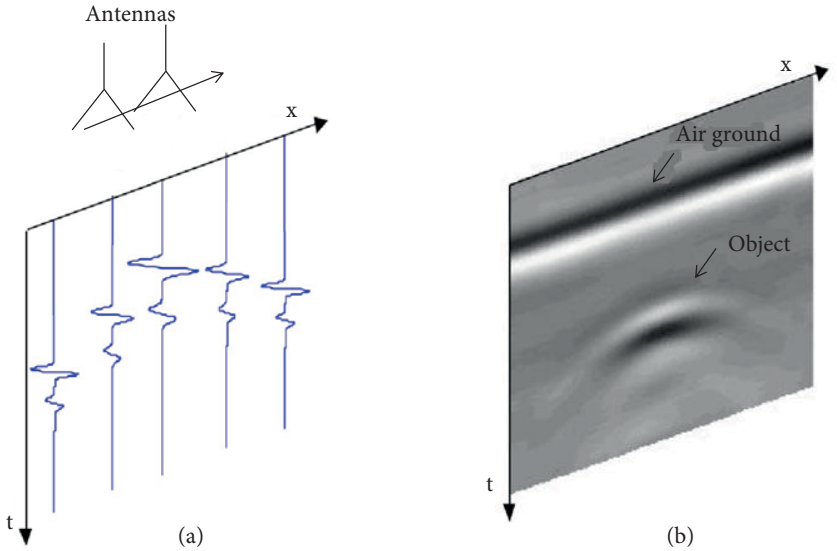

Figure 3. **(a)** Representation of GPR B-scan data, **(b)** hyperbolic response due to a single point reflector in B-scan data [34].

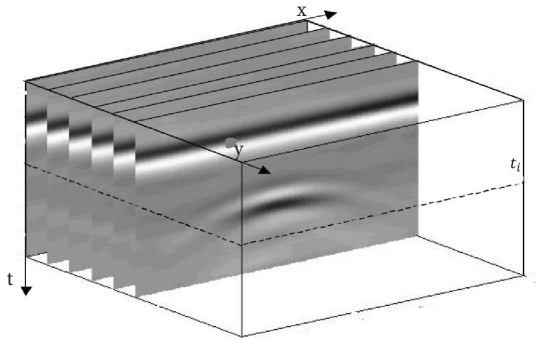

Figure 4. Representation of GPR C-scan data that are a collection of multiple B-scans [34].

3. GPR imaging techniques

3.1. Standard backprojection

Standard backprojection (SBP) is a space-time domain algorithm that performs matched filtering of the synthetic aperture radar for each point in the space domain. The impulse response of the data acquisition

process is a spatially variant hyperbolic surface. The SBP algorithm implements the matched filtering as a coherent summation along all such hyperbolas for every pixel in the image. With an infinite aperture path, the SBP can be represented as:

$$f(x_n, y_n, z_n) = \iiint_{-\infty}^{\infty} d(u_x, u_y, t)\delta\left(t - \frac{2}{c}\sqrt{z_n^2 + (y_n - u_y)^2 + (x_n - u_x)^2}\right) dt du_x du_y \tag{1}$$

where d (u_x, u_y, t) is the A-scan data collected at point (u_x, u_y) and f (x_n, y_n, z_n) is the reconstructed 3D image. SBP is a computationally complex algorithm. For 2D processing of an $N \times N$ image with N scan positions, the algorithm performs $O((N^3)$ computations. For 3D processing of an $N \times N \times N$ volume with N^2 scan positions, the computational complexity increases to $O(N^5)$.

Although the SBP is given in the time domain in Eq. (1), similar correlation-based ideas can be applied. F-K migration or Stolt migration [35] is one of the methods that can be applied in the frequency domain. In this technique the data is transformed to frequency-k space using Fourier transforms in each time and spatial dimensions. Stolt interpolation is applied in the frequency domain and the inverse Fourier transform is applied to obtain the 3D spatial domain. The procedure of F-K migration is briefly given in Figure 5. Although this method is comparably faster than backprojection, it can be only applied for a homogeneous medium.

3.2. Sparsity-based imaging

Sparsity-based GPR imaging techniques depend on the compressive sensing theory. CS techniques assume that the target space is sparse, which can be accepted in applications such as landmine detection.

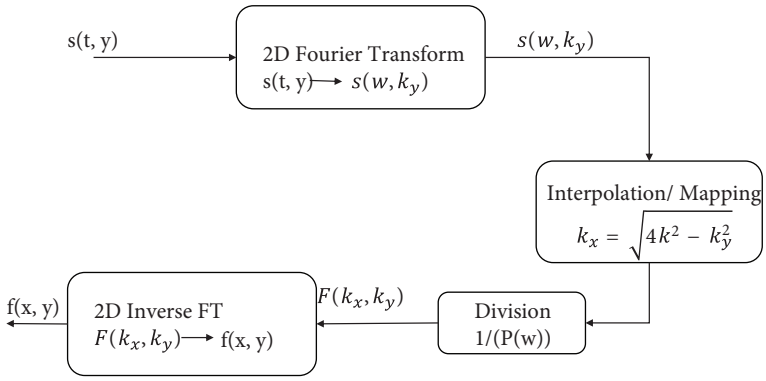

Figure 5. F-K migration method.

CS imaging needs a linear relation with the measurements and the sparsity domain to invert the under-determined linear system. Such a linear relation can be stated as:

$$d(u_x, u_y, f) = \psi\pi_T(x, y, z) \tag{2}$$

In Eq. (2), d (ux, uy, f) is the space frequency measurements, and $\pi_T(x, y, z)$ is the target space and is the operator defining the transform between two spaces. CS needs to discretize the continuous target space, which is in $[x_i, x_f] \times [y_i, y_f] \times [z_i, z_f]$, to construct a linear forward model ψ. Here (x_i, y_i, z_i) and (x_f, y_f, z_f) denote the initial and final positions of the target space to be imaged. After discretization $B = \{\pi_1, \pi_2, \ldots, \pi_N\}$, points are obtained where each π_j is a 3D vector $[x_j; y_j; z_j]$. The model data for each frequency/time

measurement at each scan position can be calculated using a forward data model for each grid point. This means that a random subset of measurements are taken at each scan position instead of taking all of them. Additionally, random spatial sampling is shown to produce correct sparse images. In this technique the data acquisition time is reduced.

It was shown in previous research about CS that stable recovery of the target space can be done by solving a convex optimization problem of the form:

$$\hat{b} = arg\min ||b||_1 \; s.t. \; \left|\left|A^T (\beta - Ab)\right|\right|_\infty < \varepsilon_1 \tag{3}$$

where **A** is the forward model, β is the compressive measurements, and variable $\boldsymbol{b}$ is the resultant target space solution. Although this type of convex optimization offers globally optimal solutions, they are computationally complex. Suboptimal solvers such as OMP are generally used to obtain faster sparse solutions. OMP does not guarantee any global optimal solution, but it is computationally very efficient, and it also has certain recovery guarantees [36] that make it a robust and preferred technique. OMP iteration relies on projecting the measurements on dictionary columns and selecting the most correlated column. The measurements are projected for the span of selected columns and at each iteration the residual is compared to a threshold. If the residual norm is small enough iterations are terminated and the least squares solution to the span of the selected columns is given as the output of OMP algorithm. Detailed algorithm steps can be found in the references cited in the introduction section.

4. Proposed 3D GPR imaging method

The goal of the proposed technique is to provide a 3D display of the sensed medium using the C-scan GPR data. To develop the proposed technique the sensed medium is first discretized into pixels as shown in Figure 6. Discretization on the continuous target space in $(x_a\,,\,x_b)$, $(y_a\,,\,y_b)$, $(z_a\,,\,z_b)$ creates $N_x\,,\,N_y\,,\,N_z$ discrete points in the x, y, and z directions, respectively. The subsurface volume is sensed with GPR on a two-dimensional grid over the surface. Assume that the antenna has $M_x \times M_y$ scan positions and at each scan position an A-scan of the GPR data is measured, resulting in a total C-scan measurement.

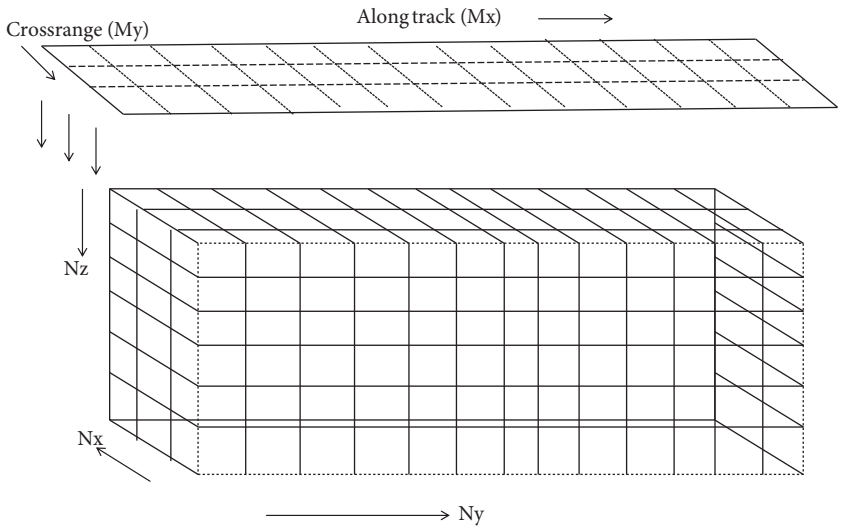

Figure 6. Discretized 3D target space and the GPR scan scenario.

The proposed method depends on the correlation of the measurements with the data model for each discrete data point. Hence, a dictionary of model data should be used. To generate the data dictionary a similar procedure as explained in Section 3.2 is followed. The data dictionary is constructed by synthesizing the GPR model data for each discrete spatial position. Discretization generates a finite set of target points $B = \{_{1,2}, \ldots, _N\}$, where $N = N_x \times N_y \times N_z$ determines the resolution and each $_j$ is a 3D vector $[x_j, y_j, z_j]$. The received signal at the GPR receiver antenna reflected from a point target can be represented as a time-delayed and scaled version of the transmitted signal $s(t\ )$ as

$$\zeta_i(t) = \frac{\sigma_p s(t - \tau_i(p))}{A_{i,p}}, \tag{4}$$

where $\tau_i(p)$ is the total round-trip delay between the antenna at the ith scan point and the target at p, σp is the reflection coefficient of the target, and $A_{i,p}$ is a scaling factor used to account for any attenuation and spreading losses. Hence, the reflected signal for a given element of B using $\sigma_p = 1$ in Eq. (4) can be calculated and placed in the corresponding column of the dictionary. The dictionary formation procedure is illustrated in Figure 7. Such a dictionary matrix is also used in sparse imaging algorithms such as CS and OMP.

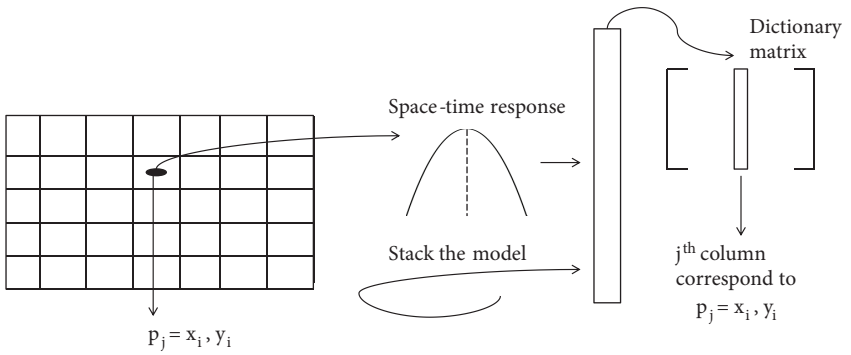

Figure 7. Construction of GPR data model dictionary matrix.

For standard 3D imaging a single column should be placed for each discrete voxel. Hence, the column number of the dictionary will be $N = N_x\ N_y N_z$. For each possible target point the sensor scans $M_x\ M_y$ spatial positions and at each scan position collects N_t measurements. Combining all these measurements makes up a single column of the dictionary and the size of each column will be $M_x M_y N_t$ by 1. In total the dictionary size will be $M_x M_y N_t$ by $N_x N_y N_z$. To emphasize the size of a dictionary for a moderate 3D GPR imaging case, an example scenario is given. In this example case, let us assume that a 1-m^3 volume is to be imaged with 2-cm grid sizes in each direction. Then N_x, N_y, N_z will be 50, making the column number of the dictionary 125,000. Assuming 100 time samples are collected on 20 $\times$ 20 scan points results in a dictionary of the size 4×10^4 by 1.25×10^5 This means a total of 5×10^9 values to be stored for the dictionary. Each point of the dictionary is a complex number. Each complex number includes real and complex numbers and each number is a float. In MATLAB, a float variable is kept in memory at 32 bits. This means that each point of the dictionary requires 64 bits or 8 bytes in the memory. Consequently, the total memory requirement of the dictionary will be $(5 \times 10^9) \times 8 = 4 \times 10^{10}$ bytes, which is approximately 37 gigabytes. Even imaging a moderate volume with practical number of measurements and scan points, storing the dictionary is very hard. Making computations with it requires dramatic computational power. Compressive sensing decreases the size of this dictionary depending on the sparsity of the sensed medium, but even with that the dictionary will still

be large. Additional information about the structure of the dictionary should be used, possibly together with compressive sensing, to get dictionary sizes that can be used in practical systems.

Our proposed technique uses the shifting structure of the data model in the scan direction to remove one of the dimensions of the dictionary. In the previous section space-time domain responses of two point-like targets at the same depth were shown. It can be seen that these responses are space-shifted versions of each other in the direction of the GPR scan. Our idea is to keep only one of these responses, and hence our goal is to construct a dictionary for just one slice of target space and represent any correlation calculations using this dictionary only.

The proposed scenario is shown in Figure 8. Normally GPR scans in the direction y from $-y_0$ to y_0 and data models for each data point in 3D space are constructed. In the proposed technique we plan to only construct the data model for the 2D target space slice shown in Figure 8, which is in the middle of the 3D target space for the scan direction, which is $y = 0$ slice.

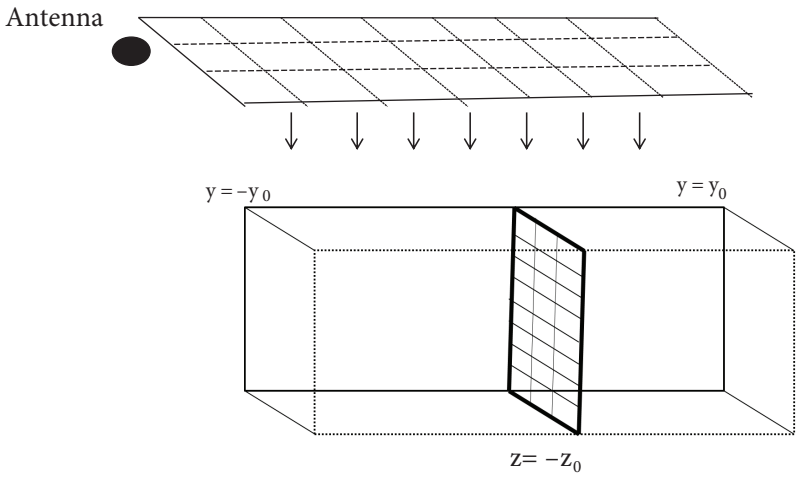

Figure 8. Dictionary dimension reduction: dictionary is created for only the corresponding target slice.

In this case the problem is how can we represent all the responses of other pixels using only this dictionary. There the shifting property of data responses comes into play. The target responses for a corresponding (x_i, z_j, 0) position of the target slice should be able to represent all 3D pixels at (x_i, z_j, y). To have such a capability first we propose to construct the data dictionary for this 2D slice at twice the length in scan direction. Although GPR scans the region from $-y_0$ to y_0 we will model the response for each target point in the 2D slice as the GPR scans the region from $-2y_0$ to $2y_0$. This will make the dictionary for the 2D slice twice as big, but since it will allow us to get rid of one whole scan dimension, gain in memory will be big. The extension of modeling in the scan direction is illustrated in Figure 9.

To understand now how we will be able to represent the responses of whole 3D volume using just the response of a 2D slice, consider first the scenarios shown in Figure 10. In the scenario shown in Figure 10 consider the data response for the target space at the $y = y_0$ slice.

In conventional 3D imaging we would create the data model for this slice as the GPR scans the region from $-y_0$ to y_0. Using the shifting property, the same data model can be achieved with the 2D dictionary created for the $y = 0$ slice; that is, the GPR sensor scans from $-2y_0$ to 0 in the y direction. Similarly for representing responses of the data slice at $y = -y_0$, GPR scans from $-y_0$ to y_0 can also be done by the proposed dictionary representation using the part from $y = 0$ to $y = 2y_0$. These two cases show that the

boundaries and data models for all other 3D pixels can be represented by using the corresponding part of the data model constructed for the 2D slice and modeled from $-2y_0$ to $2y_0$.

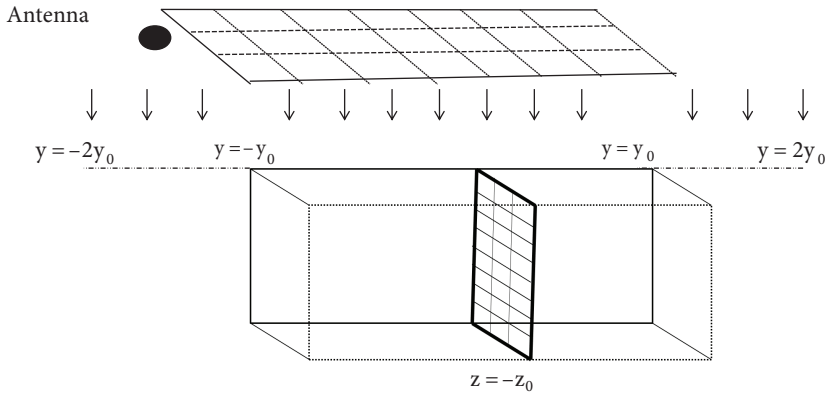

Figure 9. Modeling twice the length in scan direction for the 2D slice target space.

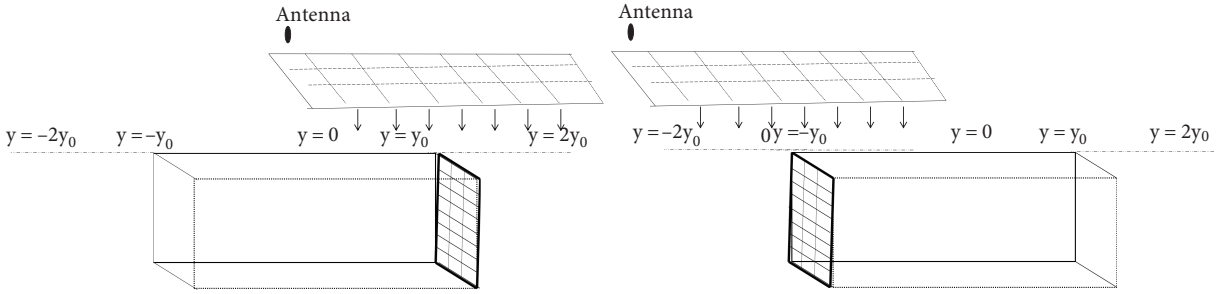

Figure 10. Parts of the GPR scan that correspond to other 3D target slices in 3D volume.

In summary, instead of creating a dictionary of size $M_xM_yN_t$ by $N_xN_yN_z$ for the conventional 3D imaging, one dimension of the dictionary is reduced by N_y but the scan size is doubled, so the size of the new dictionary is now 2 $M_xM_yN_t$ by N_xN_z. Hence, the total dictionary memory is reduced by $N_y/2$ times. Since construction of the dictionary is changed, evaluation of correlations for all 3D voxels using this new dictionary should also change. The next subsection details constructing the 3D image using the new reduced dictionary.

4.1. 3D imaging using the new reduced dictionary

Our goal is to construct the same 3D image as standard backprojection does using this new reduced dictionary. To do so we need to correlate the measurements with the dictionary, but now we do not have the data models for all 3D voxels. The measurement size is $M_xM_yN_t$ by 1 but the size of our dictionary columns are twice that as 2 $M_xM_yN_t$. This is illustrated in Figure 11. The jth column of the dictionary corresponds to points having $(x_j,\ z_j)$ with varying y values. The column part from 1 to $M_xM_yN_t$ of this column has the data model for point $(x_j,\ z_j,\ y_0)$, and the column part of 2 to $M_x\ M_yN_t + 1$ corresponds to target $(x_j,\ z_j,\ y_0 - \Delta y)$ and shifts like this until the column part of $M_xM_yN_t\ +\ 1$ to 2 $M_xM_yN_t$ that will correspond to target $(x_j,$ $z_j,\ -y_0)$. We need to correlate the measurement with these corresponding column parts to create the related correlation value that will be the voxel image value in the 3D image. Interestingly, calculating this correlation for all y values for a specific (x,z) position is only the convolution of the measurements with the corresponding

column of the proposed dictionary. Thus, the only thing to create the 3D image with the proposed method is to convolve the measurements with each column of the dictionary.

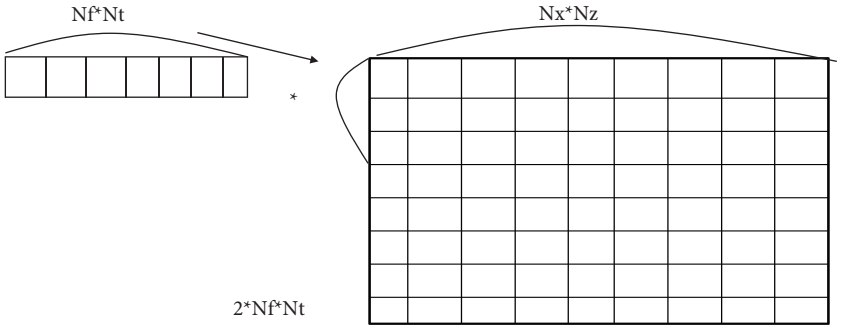

Figure 11. Proposed dictionary and the measurement vector sizes. Correlation is done by convolving the measurement vector with each column of dictionary.

In classical backprojection for 3D imaging, the computation requires $M_xM_yN_t$ multiplications and additions for each column. Taking into account having $N_xN_yN_z$ number of columns for the standard dictionary, the total number of multiplications and additions will be $M_xM_yN_tN_xN_yN_z$. In the proposed case, N_xN_z times a convolution should be applied. The convolution calculations can be applied with FFT which will further reduce the computational complexity. The proposed technique is also suitable for the OMP algorithm. In that case, the dictionary will be further reduced due to a low number of random measurements in both time/frequency or space and the proposed convolution-based technique calculates the correlation values that will also be required in each OMP iteration. In the next section, simulation results for 3D imaging and comparisons for memory and computational complexity are given.

5. Experimental results

In this section, a 3D GPR data acquisition system is simulated and the proposed imaging method is tested. To do this a two-layer stepped frequency continuous wave GPR system is modeled. Start frequency of the system is chosen as 0.5 GHz, stop frequency is chosen as 5.5 GHz, and step frequency is chosen as 80 MHz. Frequency length (M_f) is thus going to be 63. Hence, at each scan position this GPR system measured 63 complex values as its measurements. The imaging volume or the 3D target space is taken to be from -0.5 m to 0.5 m in x, -1 m to 1 m in y, and 0 m to -1 m in the z axis. In each axis the target space is discretized by 2-cm step sizes creating a pixel volume of $2 \times 2 \times 2$ cm^3. This discretization creates 51 points in the x and z directions and 101 points in the y direction. In simulation, three point targets are placed at (0, –0.25, –0.13), (0, 0.44, –0.16), and (0, 0.76, –0.49) positions. The GPR data are simulated with a signal to noise ratio of 20 dB using a rectangular grid over the surface as the scan positions. The true 3D target space is shown in Figure 12a.

As the proposed method suggests, only the dictionary for the $y = 0$ slice is constructed assuming that the GPR scans from -2 m to 2 m in the y direction. The obtained 3D image after applying the proposed method is shown in Figure 12b. All 3 targets can be seen at their correct locations. The shown image is an isosurface image of the 3D volume. The proposed technique saved nearly 50 times the memory for this specific example as compared to standard backprojection.

To compare the memory performance of the classical backprojection and the proposed method, the grid size used in discretization of the 3D target space is changed and the required dictionary memories for both

methods are compared. The obtained results are shown in Figure 13a. It can be seen in simulation results that the proposed method requires much lower memory to save the dictionary as compared to backprojection for all grid sizes. It can be also observed that decreasing grid size dramatically increases memory requirement of backprojection while this increase is more limited for the proposed technique.

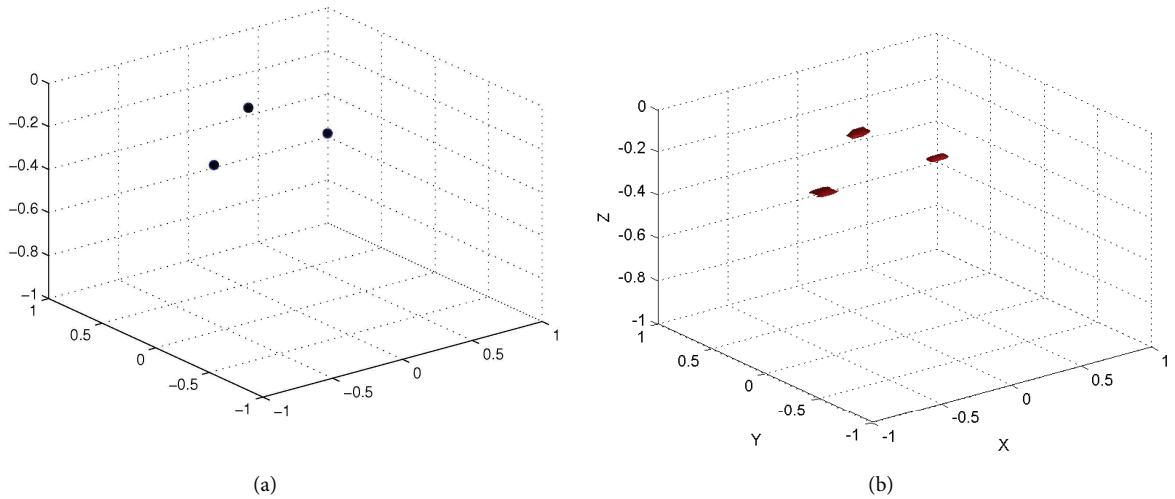

Figure 12. (a) True target space, (b) constructed 3D image with the proposed technique.

Another advantage of the proposed method is the computational complexity. The computational load depends on the discrete target number or correspondingly the column number of the dictionaries. Hence, the computational load of both methods is compared as the number of spatial points, N, is changed. The computational comparison is shown in Figure 13b and it can be seen that the proposed method provides a computational advantage in constructing the 3D image due to inherent convolution calculations.

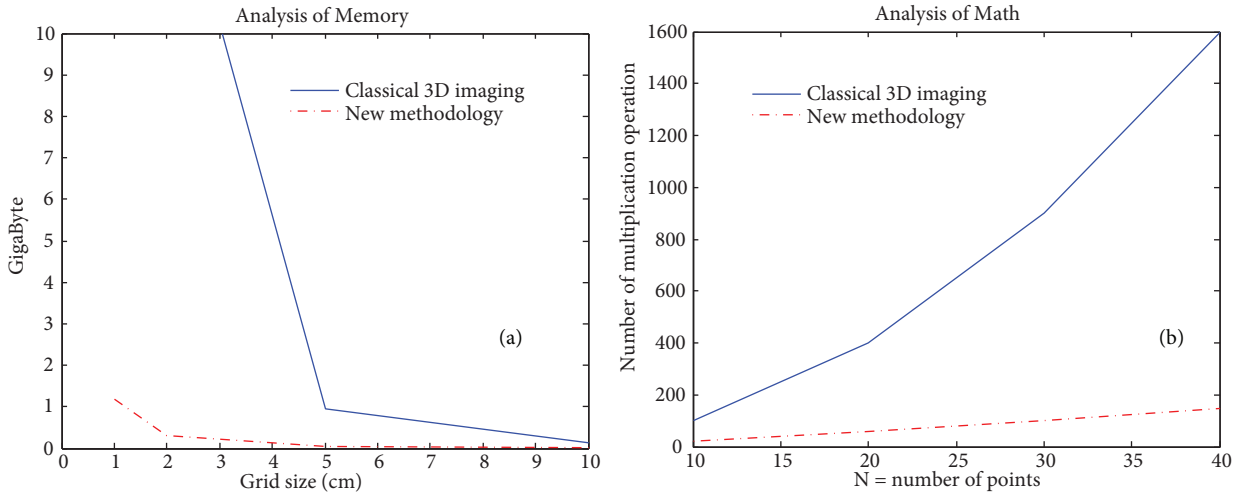

Figure 13. Comparison of standard backprojection and the proposed method in terms of (a) memory requirement and (b) computational load.

6. Conclusions

A new technique for 3D imaging for time domain or stepped frequency GPR systems is presented. Compared to the conventional backprojection, which requires creating the data model for each discrete target point in 3D space, the proposed technique only creates a dictionary for one slice of the target space, creating a dimension reduction in the scanning direction of the GPR system by using the shifting property of GPR data models in the down-track scan direction. Similar ideas can also be applied to the cross-track direction as well. In this way the huge memory requirements for 3D GPR imaging are significantly reduced. The proposed method is also suitable to be used for sparse representation algorithms such as OMP, and dictionary reduction advantages of OMP such as random time or space measurements can be incorporated with the proposed method. The proposed technique also decreases the computational load of the 3D imaging by using convolution-based correlation calculations. Simulation results show that correct 3D subsurface images could be obtained with the proposed technique. As a future work, we think that combining the proposed technique with the data reduction ideas of compressive sensing might result in more practical and successful 3D imaging systems.

Acknowledgments

This study was supported by both a TÜBİTAK Career Research grant with agreement number 109E280 and within the FP7 Marie Curie IRG Grant with grant agreement number PIRG04-GA-2008-239506.

References

[1] H.M. Jol, Ground Penetrating Radar Theory and Applications, Elsevier, Amsterdam, 2009.

[2] M.G. Amin, Through-the-Wall Radar Imaging, CRC Press, Boca Raton, 2010.

[3] D.J. Daniels, "Surface-penetrating radar", Electronics and Communication Engineering Journal, Vol. 8, pp. 165–182, 1996.

[4] J. Groenenboom, A. Yarovoy, "Data processing and imaging in GPR system dedicated for landmine detection", Subsurface Sensing Technologies and Applications, Vol. 3, pp. 387–402, 2002.

[5] K. Kim, A.C. Gurbuz, J.H. McClellan, W.R. Scott Jr, "A multi-static ground-penetrating radar with an array of resistively loaded vee dipole antennas for landmine detection", Detection and Remediation Technologies for Mines and Minelike Targets X, Proceedings of the SPIE, Vol. 5794, pp. 495–506, 2005.

[6] S. Hubbard, C. Jinsong, K. Williams, Y. Rubin, J. Peterson, "Environmental and agricultural applications of GPR", Proceedings of the 3rd International Workshop on Advanced Ground Penetrating Radar, pp. 45–49, 2005.

[7] A.C. Gurbuz, J.H. McClellan, W.R. Scott Jr, G.D. Larson, "Seismic tunnel imaging and detection", IEEE Conference On Image Processing, pp. 3229–3232, 2006.

[8] E.J. Baranoski, "Through-wall imaging: historical perspective and future directions", Journal of the Franklin Institute, Vol. 345, pp. 556–569, 2008.

[9] N. Metje, P.R. Atkins, M.J. Brennan, D.N. Chapman, H.M. Lim, J. Machell, J.M. Muggleton, S. Pennock, J. Ratcliffe, M. Redfern, C.D.F. Rogers, A.J. Saul, "Mapping the underworld - state of the art review", Tunneling and Underground Space Technology, Vol. 22, pp. 568–586, 2007.

[10] G. Grandjean, J.C. Gourry, A. Bitri, "Evaluation of GPR techniques for civil-engineering applications: study on a test site", Journal of Applied Geophysics, Vol. 45, pp. 141–156, 2000.

[11] A.C. Gürbüz, "Line detection with adaptive random samples", Turkish Journal of Electrical Engineering and Computer Science, Vol. 19, pp. 21–32, 2011.

[12] J. Leckebusch, "Ground-penetrating radar: a modern three-dimensional prospection method", Archaeologica Prospection, Vol. 10, pp. 213–240, 2003.

[13] M. Lualdi, L. Zanzi, G. Sosio, "A 3D GPR survey methodology for archaeological applications", Proceedings of the 11th International Conference on Ground Penetrating Radar, Columbus, OH, USA, 2006.

[14] M. Grasmueck, R. Weger, H. Horstmeyer, "Full-resolution 3D GPR imaging", Geophysics, Vol. 70, pp. K12–K19, 2006.

[15] J. Song, Q.H. Liu, P. Torrione, L. Collins, "Two-dimensional and three-dimensional NUFFT migration method for landmine detection using ground-penetrating Radar", IEEE Transactions on Geoscience and Remote Sensing, Vol. 44, pp. 1462–1469, 2006.

[16] E.M. Johansson, J.E. Mast, "Three dimensional ground penetrating radar imaging using a synthetic aperture time-domain focusing", Proceedings of the SPIE Conference on Advanced Microwave and Millimeter Wave Detectors, Vol. 2275, pp. 205–214, 1994.

[17] R. Stolt, "Migration by Fourier transform", Geophysics, Vol. 43, pp. 23–48, 1978.

[18] H. Gan, W.C. Chew, "A discrete BCG-FFT algorithm for solving 3D inhomogeneous scatterer problems", Journal of Electromagnetic Waves and Applications, Vol. 9, pp. 1339–1357, 1995.

[19] A.C. Gurbuz, J.H. McClellan, W.R. Scott Jr, "Subsurface target imaging using a multi-resolution 3D quadtree algorithm", Detection and Remediation Technologies for Mines and Mine-like Targets X, Proceedings of the SPIE, Vol. 5794, pp. 1172–1181, 2005.

[20] A.C. Gurbuz, J.H. McClellan, W.R. Scott Jr, "Imaging of subsurface targets using a 3D quadtree algorithm", ICASSP, Vol. 4, pp. 1105–1108, 2005.

[21] D.L. Donoho, "Compressed sensing", IEEE Transactions on Information Theory, Vol. 52, pp. 1289–1306, 2006.

[22] E. J. Candes, J. Romberg, T. Tao, "Robust uncertainty principles: exact signal reconstruction from highly incomplete frequency information", IEEE Transactions on Information Theory, Vol. 52, pp. 489–509, 2006.

[23] E. Candes, J. Romberg, T. Tao, "Stable signal recovery from incomplete and inaccurate measurements", Communications on Pure and Applied Mathematics, Vol. 529, pp. 1207–1223, 2006.

[24] D.L. Donoho, M. Elad, V.N. Temlyakov, "Stable recovery of sparse overcomplete representations in the presence of noise", IEEE Transactions Information Theory, Vol. 52, pp. 6–18, 2006.

[25] A.C. Gurbuz, J.H. McClellan, W.R. Scott Jr, "Compressive sensing for GPR imaging", Asilomar Conference on Signals, Systems, and Computers, pp. 2223–2227, 2007.

[26] A.C. Gurbuz, J.H. McClellan, W.R. Scott Jr, "A compressive sensing data acquisition and imaging method for stepped frequency GPRs", IEEE Transactions on Signal Processing, Vol. 57, pp. 2640–2650, 2009.

[27] A.C. Gurbuz, J.H. McClellan, W.R. Scott, "Compressive sensing for subsurface imaging using ground penetrating radars", Signal Processing, Vol. 89, pp. 1959–1972, 2009.

[28] Y. Yoon, M.G. Amin, "Imaging of behind the wall targets using wide-band beamforming with compressive sensing", Statistical Signal Processing, pp. 93–96, 2009.

[29] J. Tropp, A. Gilbert, "Signal recovery from random measurements via orthogonal matching pursuit", IEEE Transactions on Information Theory, Vol. 53, pp. 4655–4666, 2007.

[30] M.A.Ç. Tuncer, A.C. Gürbüz, "Analysis of orthogonal matching pursuit based subsurface imaging for compressive ground penetrating radars", Turkish Journal of Electrical Engineering and Computer Science, Vol. 20, pp. 979–989, 2012.

[31] K. Krueger, J.H. McClellan, W.R. Scott Jr, "Dictionary reduction technique for 3D stepped-frequency GPR imaging using compressive sensing and FFT", Proceedings of the SPIE, Vol. 8365, p. 83650Q, 2012.

[32] K. Krueger, J.H. McClellan, W.R. Scott Jr, "3-D imaging for ground penetrating radar using compressive sensing with block-Teoplitz structures", IEEE 7th Sensor Array and Multichannel Signal Processing Workshop, pp. 229–232, 2012.

[33] M. Duman, A.C. Gurbuz, "Faster 3D GPR imaging using 2D dictionaries with applications to sparse reconstruction", ICECCO Conference, 2012.

[34] B. Scheers, "Ultra-wideband ground penetrating radar, with application to the detection of anti personnel landmines", Royal Military Academy, Brussels, 2001.

[35] W.A. Burnett, R.J. Ferguson, "Reversible Stolt migration", CREWES Research Report, 2008.

[36] J. Wang, B. Shim, "On the recovery limit of sparse signals using orthogonal matching pursuit", IEEE Transactions on Signal Processing, Vol. 60, pp. 4973–4976, 2012.